Supplementary Material (ESI) for Soft Matter

Simultaneous Microfluidic Generation of Droplets with Different Dimensions

Wei Li,[a] Edmond W. K. Young,[b] Minseok Seo ,[a] Zhihong Nie,[a] Piotr Garstecki, [d]
Craig A. Simmons, [b] and Eugenia Kumacheva*[a,c,e]

[a] Department of Chemistry, University of Toronto,
80 St. George Street, Toronto, Ontario, M5S 3H6, Canada.

[b] Department of Mechanical & Industrial Engineering, University of Toronto,
5 King's College Road, Toronto, Ontario, M5S 3G8, Canada

[c] Department of Chemical Engineering and Applied Chemistry, University of Toronto,
200 College Street, Toronto, Ontario, M5S 3E5, Canada.

[d] Institute of Physical Chemistry, Polish Academy of Sciences,
Kasprzaka 44/52, 01-224 Warsaw, Poland

[e]Institute of Biomaterials and Biomedical Engineering, 164 College Street, University of Toronto,
Toronto, Ontario,M5S 3G9, Canada.

Fax,Tel:416-978-3576; E-mail: ekumache@chem.utoronto.ca

1. Calculation of volumes of droplets.

The volume of an undeformed spherical droplet (Fig. 1a) is given by $V= 4/3\ \pi R^3$ where R is the radius of the droplet. The volume of the droplet segment in Fig. 1b is $V_s =1/3\ \pi h`^2\ (3R-h`)$ where h` is the height of the segment. The volume of the disk with the height h (h =2R-h`) is thus equal to $(\pi/12)[2D^3-(D-h)^2\ (2D+h)]$ where D is the diameter of the disk (Fig. 1c).

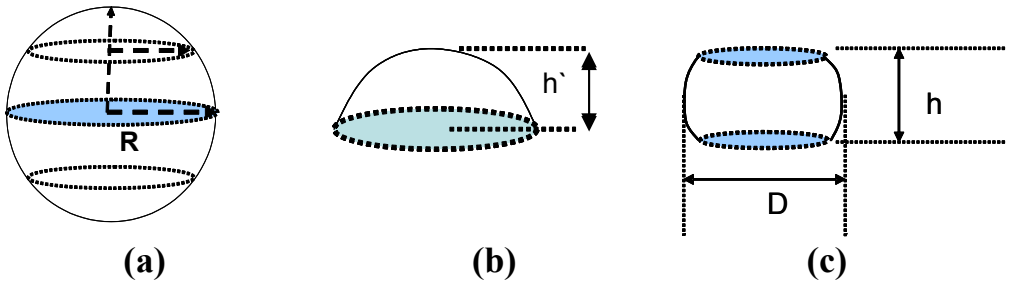

Fig. 1. Schematics used for the calculation of the volumes of droplets obtained in multiple droplet generators.

Table 1. Diameters of droplets and coefficients of variance (CV) of droplets obtained in four non-integrated FFDs

	FFD-1	FFD-2	FFD-3	FFD-4	Total population of droplets		Q_B (mL/hr)	Q_A (mL/hr)
Width of orifice (μm)	50.7±1.0	50.8±1.0	48±1.0	48.8±1.0				
D_m (μm) / CV(%)	105.5/1.4	103.2/1.5	102.2/1.4	104.1/1.2	103.8	1.7	0.25	0.005 (T1) (T2) (T3)
	104.3/1.3	104.6/1.3	103.1/1.2	103.9/1.3	104.0	1.5		
	105.0/1.3	103.6/1.4	102.9/1.5	102.2/1.6	103.4	1.9		
	112.1/1.3	113.0/1.0	112.9/1.2	111.2/1.4	112.3	1.5		0.0125 (T1) (T2) (T3)
	112.8/1.6	114.2/1.1	111.2/1.5	110.6/1.1	112.2	1.6		
	114.2/1.5	112.6/1.3	110.6/1.5	114.3/1.2	112.9	1.7		
	132.6/1.1	132.4/0.9	129.7/1.0	130.5/1.1	131.3	1.6		0.020 (T1) (T2) (T3)
	130.6/1.3	135.1/1.0	130.6/0.9	133.2/0.9	132.4	1.4		
	131.5/1.1	134.3/1.2	132.9/0.9	130.6/1.1	132.3	1.6		
	91.9/1.1	93.8/1.4	95.3/1.4	93.3/1.6	93.6	1.9	0.30	0.005 (T1) (T2) (T3)
	91.0/1.2	92.6/1.6	93.6/1.5	92.6/1.2	92.5	1.7		
	90.5/1.4	93.5/1.5	93.1/1.1	93.7/1.2	92.7	1.6		
	107.2/1.3	109.3/1.4	107.0/1.3	106.5/1.5	107.5	1.6		0.005 (T1) (T2) (T3)
	108.2/1.5	108.6/1.2	107.9/1.2	106.6/1.4	107.8	1.8		
	106.9/1.2	109.9/1.4	105.4/1.4	104.9/1.1	106.8	2.0		
	116.7/1.1	118.4/1.0	115.9/1.1	116.7/1.2	116.9	1.7		0.0125 (T1) (T2) (T3)
	116.2/1.4	116.5/1.2	116.8/1.4	115.5/1.1	116.3	1.6		
	115.2/1.3	117.2/1.1	118.3/1.5	114.3/1.5	116.3	1.8		
	81.1/1.5	82.3/1.6	80.4/1.7	80.8/1.4	81.2	1.9	0.35	0.005 (T1) (T2) (T3)
	80.6/1.4	82.9/1.4	80.1/1.5	79.3/1.6	80.7	2.0		
	82.0/1.6	81.6/1.3	81.6/1.2	79.0/1.7	81.1	1.9		
	96.9/1.3	98.1/1.5	98.5/1.0	97.2/1.5	97.7	1.6		0.0125 (T1) (T2) (T3)
	95.3/1.2	97.5/1.4	97.6/1.5	98.9/1.2	97.3	1.7		
	97.2/1.5	97.0/1.6	96.9/1.4	97.7/1.4	97.2	1.7		
	105.6/1.5	107.2/1.3	105.8/1.3	106.3/1.4	106.2	1.8		0.020 (T1) (T2) (T3)
	105.8/1.4	106.4/1.6	106.8/1.2	104.9/1.6	106.0	1.9		
	104.3/1.2	105.9/1.5	108.0/1.6	103.7/1.6	105.5	2.0		
	73.5/1.7	76.5/1.6	74.2/1.8	73.1/1.6	74.3	2.1	0.40	0.005 (T1) (T2) (T3)
	72.4/1.6	75.5/1.6	70.6/1.2	71.2/1.4	72.4	1.8		
	73.9/1.7	74.9/1.7	72.6/1.3	70.6/1.5	73.0	1.9		
	83.5/1.8	85.6/1.6	83.5/1.5	86./1.4	84.7	1.7		0.0125 (T1) (T2) (T3)
	82.1/1.6	86.3/1.5	85.3/1.1	85.5/1.2	84.8	1.7		
	83.1/1.4	84.9/1.6	86.3/1.6	84.2/1.5	84.6	1.9		
	92.9/1.6	94.9/1.6	91.9/1.2	93.7/1.4	93.4	1.8		0.020 (T1) (T2)
	91.3/1.6	93.0/1.3	93.1/1.1	91.1/1.4	92.1	1.8		

	90.8/1.5	94.1/1.6	92.7/1.5	90.6/1.5	92.1	1.8	(T3)

T1, T2 and T3 are three trials under the same flow rate Q_A and Q_B.

2. Reproducible formation of droplets in the QDGs

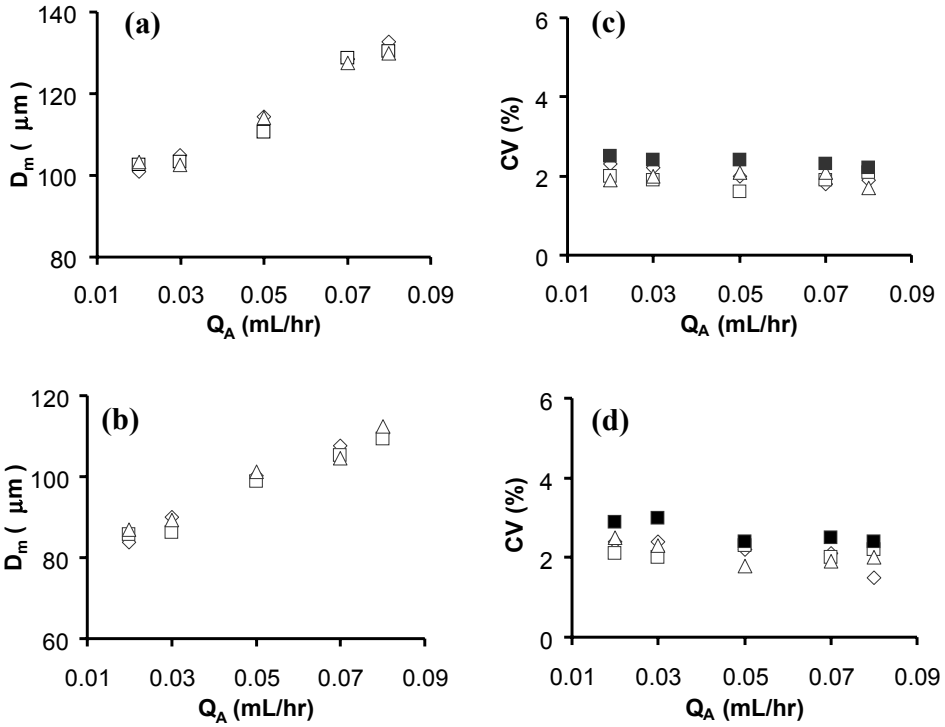

Fig. 2. (a,b) Variation in mean diameter of droplets generated in FFD-2, plotted as a function of the flow rate, Q_A, of the droplet phase at (a): Q_B= 1.0 mL / hr and (b): Q_B= 1.4 mL/hr. (c, d) Variation in polydispersity of droplets produced in FFD-2 in three consecutive emulsification experiments (open symbols) and of the total population of droplets (■). Orifice width of FFD-2: 50.8±1.0 µm.

Fig. 2a, b shows a representative change in the mean diameter of droplets obtained in FFD-2, plotted as a function of the flow rate of the droplet phase, Q_A. In the same range of flow rates as in Fig. 3 in the main text of the article, the difference in mean diameter of droplets formed in the successive emulsification experiments was from 1 to 5 µm. Fig. 2c, d shows that the value of the CV of droplets generated in each emulsification experiment was in the range from 1.6 to 2.5 %, while the CV of the entire collection of droplets produced in three experiments did not exceed 3%.

3. Redistribution of volumes of liquids in the QDG with varying orifice widths

The variation in dimensions of droplets generated in parallel flow-focusing devices (FFDs) with varying orifice widths can partly be attributed to the uneven splitting of volumes of liquids in the different paths of the QDG, due to the differences in the hydrodynamic path resistances. The QDG is a multichannel network of parallel fluidic paths, with each path consisting of rectangular channel sections of varying lengths and cross-sectional widths that are connected in series. The flow rates in corresponding sections of separate paths are not equal because the differences in orifice widths are coupled through the interconnected channels.

Determining the flow rates of the fluid streams just prior to entrance into their respective orifices can elucidate the effect of varying orifice widths on the size of droplets. To demonstrate this effect, we analyzed a significantly simpler problem of flow of a *single* phase in all sections of the microchannel network. All other effects related to the multiphase flow, the properties of liquids, or other non-geometric considerations required more sophisticated approaches that were beyond the scope of the present analysis. For convenience, we have continued to use subscripts A and B to distinguish between the streams of the *same* liquid entering the orifice from top Sheet 3 (stream A) and intermediate Sheet 2 (stream B) (Figure 3). The purpose of this distinction was to track the volume fraction of stream A passing through the different orifices and obtain theoretical predictions of flow rate ratios that can be readily compared to our experimental results.

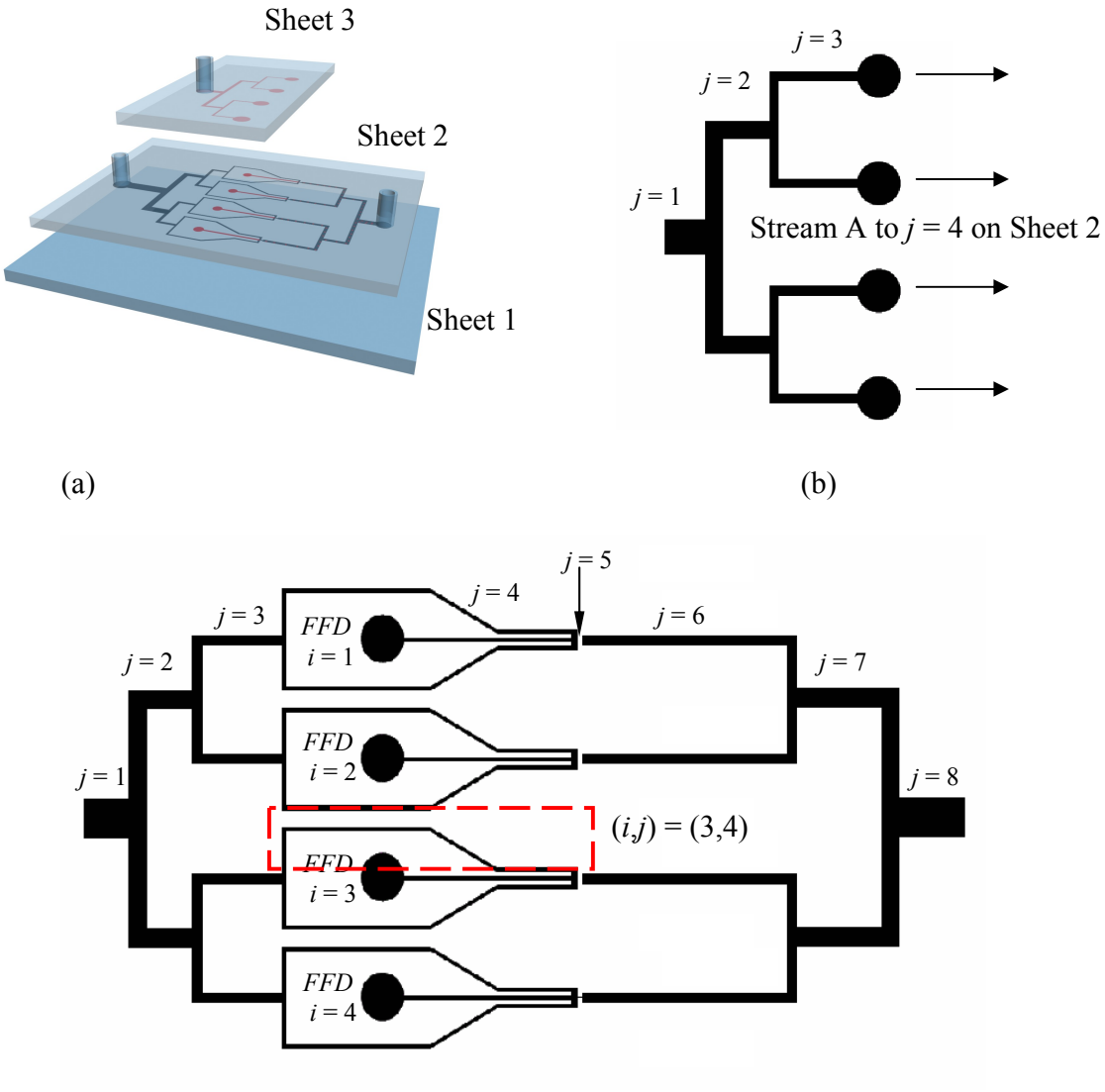

Fig. 3 (a) 3D illustration of QDG. (b) Index convention (*i*,*j*) for microchannels fabricated in Sheet 3, (c) Index convention (*i*,*j*) for microchannels fabricated in Sheet 2.

Each channel section of the network was designated by an index pair (*i*,*j*), where *i*

represented the FFD to which the section belongs, and j represented the position of that section within the i^{th} FFD. In Fig. 3, four FFDs are marked with i changing from 1 to 4 (from top to bottom in Fig. 3c). Each FFD consists of two identical paths from the inlet to the outlet for stream B, each containing eight microchannel sections j = 1 to 8 (including the orifice j = 5), and one path for stream A containing four microchannel sections j = 1 to 4 (where j = 4 for stream A resides in intermediate sheet 2). For example, the microchannel section outlined with a dotted line in Fig. 3c is designated as section (3,4), since it belongs to the third FFD from the top, and is the fourth distinct section having a different length and cross-sectional width. We note that this scheme results in the same index pair (i,4) being applied to the two channel sections in each FFD where j = 4, i.e., two streams B leading directly into the orifice. Furthermore, several sections may have multiple index pairs, if the section is connected to more than one FFD (e.g. the inlet). From the developments below it will become clear that these anomalies in the notations are permissible, given the correct formulation.

We denote the volumetric flow rate in section (i,j) as $Q^{(i,j)}$, the velocity in (i,j) as $V^{(i,j)}$, and the head loss in (i,j) as $h_f^{(i,j)}$. Fig. 4 shows a close-up view of the orifice region for the i^{th} FFD. When no subscript is used, the term represents a flow parameter in a section downstream of the orifice where streams A and B merge.

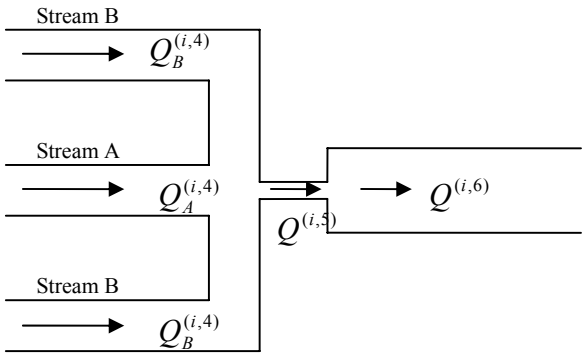

Fig. 4 Notations used for flow rates of liquids near the orifice region for the i^{th} FFD.

To proceed with the analysis, we followed the following rules that apply to viscous duct flow through channel networks[1]: (1) the total flow rate entering a section is equal to the total flow rate exiting the section; (2) the total head loss $\Delta h_f^{(i)}$ of a single fluidic path in the i^{th} FFD is equal to the sum of the head losses in each section *connected in series* within that path, and (3) the total head loss between the paths *connected in parallel* must be equal. Thus for the first FFD (FFD-1) of the quadra-droplet generator, we obtained the following equations:

$$Q_A^{(1,3)} = Q_A^{(1,4)} \tag{1}$$

$$Q_A^{(1,2)} = Q_A^{(1,3)} + Q_A^{(2,3)} \tag{2}$$

$$Q_A^{(1,1)} = Q_A^{(1,2)} + Q_A^{(3,2)} \tag{3}$$

$$Q_B^{(1,3)} = 2Q_B^{(1,4)} \tag{4}$$

$$Q_B^{(1,2)} = Q_B^{(1,3)} + Q_B^{(2,3)} \tag{5}$$

$$Q_B^{(1,1)} = Q_B^{(1,2)} + Q_B^{(3,2)} \tag{6}$$

$$Q^{(1,5)} = Q_A^{(1,4)} + 2Q_B^{(1,4)} \tag{7}$$

$$Q^{(1,6)} = Q^{(1,5)} \tag{8}$$

$$Q^{(1,7)} = Q^{(1,6)} + Q^{(2,6)} \tag{9}$$

$$Q^{(1,8)} = Q^{(1,7)} + Q^{(3,7)} \tag{10}$$

Eqns (1)-(3) apply to stream A before the orifice. Eqn (1) shows that the flow rate, $Q_A^{(1,3)}$, of stream A leaving Sheet 3, is equal to the flow rate, $Q_A^{(1,4)}$, entering Sheet 2. Eqns (4)-(6) apply to stream B before the orifice. Eqn (4) shows that the flow rate of stream B exiting the section where j = 3 is equally divided between the two downstream channels (j = 4), since they are paths with identical geometries. Eqn (7) states that the flow rate in the orifice $Q^{(1,5)}$ is equal to the combined flow rates of the incoming streams A and B. Finally, eqns (8)-(10) apply to the flow rates downstream of the orifice.

Similar equations apply to all four FFDs (and in principle, generalizations can be made for any number of FFDs connected in parallel). Close inspection reveals that the flow rates in all channel sections can be expressed in terms of $Q_A^{(i,4)}$ and $Q_B^{(i,4)}$ alone, for i = 1 to 4. Therefore, once these eight flow rates are solved, the flow rates in the entire channel network can be determined.

To solve $Q_A^{(i,4)}$ and $Q_B^{(i,4)}$, we apply rules 2 and 3 stated above. Head loss in any channel section (i,j) can be expressed as

$$h_f^{(i,j)} = \left(f^{(i,j)} \frac{L^{(i,j)}}{D_h^{(i,j)}} \right) \frac{\left(V^{(i,j)}\right)^2}{2g} \tag{11}$$

where f is the Darcy friction factor, L is the channel length, D_h is the hydraulic diameter of the rectangular cross section (equal to four times the cross-sectional area divided by

the wetted perimeter), and g is the acceleration of gravity, g = 9.81 m/s^2. For rectangular cross sections, f can be calculated using the well-cited formulation of Shah and London[2],

$$f \cdot \mathrm{Re} = 96\left(1 - 1.3553\alpha + 1.9467\alpha^2 - 1.7012\alpha^3 + 0.9564\alpha^4 - 0.2537\alpha^5\right) \quad (12)$$

where α is the aspect ratio of the channel (α is calculated as the ratio of height and width, or the inverse, whichever is smaller). We note that although discrepancies between eqn (12) and experimental data on frictional flows in microchannels had been reported, Steinke and Kandlikar[3] recently confirmed the validity of this equation for microfluidic channels by attributing past inconsistencies to the lack of attention to the entrance and exit effects at the microscale.

For a single fluidic path of the i^{th} FFD starting from inlet A in Sheet 3, the total head loss $\Delta h_{f,A}^{(i)}$ is given by

$$\Delta h_{f,A}^{(i)} = \sum_{j=1}^{4} h_{f,A}^{(i,j)} + \sum_{j=5}^{8} h_f^{(i,j)} \quad (13)$$

Likewise, for a single fluidic path of the i^{th} FFD starting from inlet B, the total head loss $\Delta h_{f,B}^{(i)}$ is

$$\Delta h_{f,B}^{(i)} = \sum_{j=1}^{4} h_{f,B}^{(i,j)} + \sum_{j=5}^{8} h_f^{(i,j)} \quad (14)$$

The second summation term from j = 5 to 8 is identical in eqn (13) and (14) because the channel sections from the orifice onward are identical in both cases. Minor losses, due to bends and elbows as well as expansions and contractions, were neglected because the large friction factors and large ratios L/D_h for the channel sections dominated the value of head loss. Eqn (13) and (14) apply to all FFDs, and since all parallel fluidic paths have the same total head loss, we obtain

$$\Delta h_{f,A}^{(1)} = \Delta h_{f,A}^{(2)} = \Delta h_{f,A}^{(3)} = \Delta h_{f,A}^{(4)} \tag{15}$$

and

$$\Delta h_{f,B}^{(1)} = \Delta h_{f,B}^{(2)} = \Delta h_{f,B}^{(3)} = \Delta h_{f,B}^{(4)} \tag{16}$$

for streams A and B, respectively.

Equations (1)-(14) can be extended to all FFDs in the system and combined with equations (15) and (16) to yield a set of equations that are solved iteratively for $Q_A^{(i,4)}$ and $Q_B^{(i,4)}$. To do so, we first assumed initial values for $Q_A^{(i,4)}$ and $Q_B^{(i,4)}$ and then calculated the total head loss in all fluidic paths using eqn (1)-(14). If the calculated head loss between parallel fluidic paths did not satisfy eqns (15) and (16), the values of $Q_A^{(i,4)}$ and $Q_B^{(i,4)}$ were adjusted by a correction factor of the form

$$\left[Q_A^{(i,4)}\right]^{n+1} = \left[Q_A^{(i,4)}\right]^{n} \times \left[\frac{\Delta h_{f,A}^{(1)}}{\Delta h_{f,A}^{(i)}} \frac{Q_A}{\sum_i Q_A^{(i,4)}}\right]^{n} \tag{17}$$

$$\left[Q_B^{(i,4)}\right]^{n+1} = \left[Q_B^{(i,4)}\right]^{n} \times \left[\frac{\Delta h_{f,B}^{(1)}}{\Delta h_{f,B}^{(i)}} \frac{Q_B}{2\times\sum_i Q_B^{(i,4)}}\right]^{n} \tag{18}$$

for streams A and B, respectively. In eqns (17) and (18), superscript *n* identifies the unadjusted value of the flow rate in section j = 4, superscript *n*+1 identifies the corrected flow rate, and Q_A and Q_B are the total flow rates of the liquids delivered to the inlets of streams A and B, respectively. The correction factor consisted of a head loss ratio and a flow rate ratio. The head loss ratio $\Delta h_f^{(1)} / \Delta h_f^{(i)}$ increased the flow rate if $\Delta h_f^{(i)}$ was lower than $\Delta h_f^{(1)}$, or decreased the flow rate if $\Delta h_f^{(i)}$ was higher than $\Delta h_f^{(1)}$. This correction

forced the head loss in the parallel paths to converge to a single value. The flow rate ratio ensured that the calculated flow rates totalled the delivered flow rates Q_A and Q_B. Note that the only difference between equations (17) and (18) is a factor of two, which accounts for the two identical paths for stream B in the section of each FFD where $j = 4$.

The experimental dimensions of the microchannels and eqns. (1)-(16) were input into an Excel spreadsheet program. The iterative procedure and Eqns. (17) and (18) were applied to solve the eight unknown flow rates, $Q_A^{(i,4)}$ and $Q_B^{(i,4)}$ for inlet flow rates of Q_A = 0.2 ml/hr and Q_B varying from 1.0 to 2.0 ml/hr (i.e., the values of Q_B/Q_A in the range from 5 to 10). These flow rates yielded solutions to the eight unknown flow rates $Q_A^{(i,4)}$ and $Q_B^{(i,4)}$. For the results presented, we assumed the properties of water for streams A and B (density of water ρ_w = 1000 kg/m^3, viscosity of water μ_w = 0.001 kg/m s).

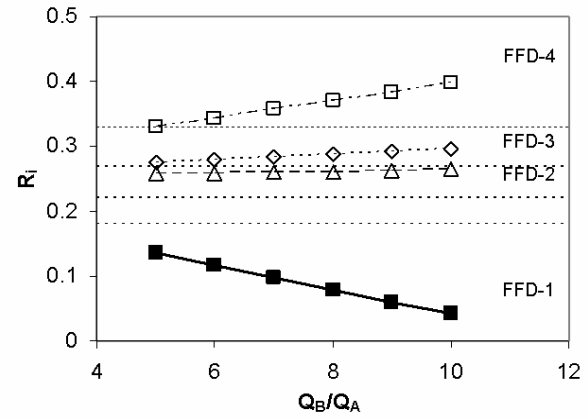

(a)

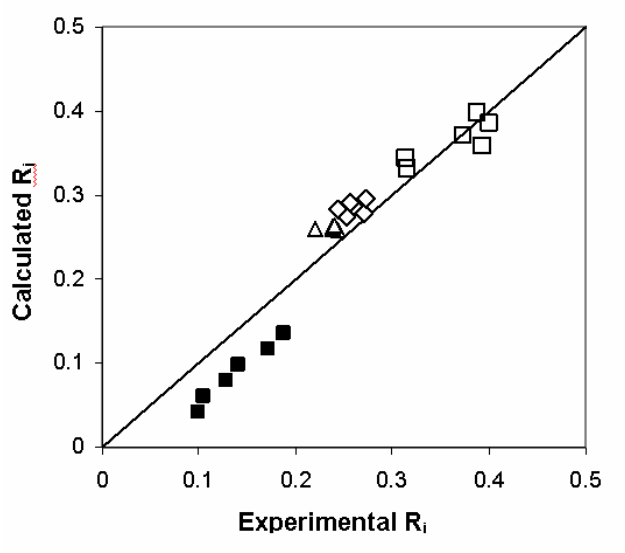

(b)

Fig. 5 (a) Variation in calculated volume fraction R_i, of stream A, in FFDs with varying orifice widths, plotted as a function of the ratio Q_B/Q_A. The horizontal dashed lines (bottom to top) represent the volume fraction of an orifice in an individual FFD (from FFD-1 to FFD-4, respectively) to the total volume of orifices in the QDG (compare with Figure 6 of main text). (b) Calculated R_i values versus experimental R_i values. The graph shows good agreement between experimental and modelled results for FFD-1 (■), FFD-2 (Δ), FFD-3 (◊) and FFD-4 (□).

Fig. 5a shows the calculated results of the volume fraction, R_i, of stream A in each FFD, plotted as a function of the ratio Q_B/Q_A. The volume fraction of droplets obtained in an individual FFD was defined as $R_i = (V_i/V_{tot})$ where Vi is the total volume of droplets produced in an individual FFD and V_{tot} is the total volume of droplets obtained in the quadra-droplet generator. These results are in good agreement with experimental data shown in Fig. 5 in the main text of the article, giving a similar trend of decreasing R_i with increasing Q_B/Q_A for FFD-1 (comprising the narrowest orifice), and increasing R_i with increasing Q_B/Q_A for FFD-4 (comprising the widest orifice).

Furthermore, in Fig. 5b a plot comparing the experimental results and the results of modellionfirms that they are in very good agreement.

As confirmation that these results were due to the microchannel geometry alone, we also performed simulations using the properties of light mineral oil (density of mineral oil ρ_o = 841 kg/m^3, viscosity of mineral oil μ_w = 0.030 kg/m s). Although head losses through the microchannels were much larger for mineral oil, due to higher viscosity, the results for volume fraction R_i as presented in Fig. 5 were identical to the results obtained with water.

Although we have only analyzed the simplified case of one-phase flow, the uneven distribution of the volume of stream A between the coupled FFDs explains the *trends* in the variation of the size of droplets obtained in the QDG. However, close examination of Fig. 5b reveals that the experimental values of R_i for FFD-1 are noticeably lower than the calculated R_i values. This discrepancy suggests that for narrow orifices, the multiphase flow, the rate-of-flow controlled breakup, and the Laplace pressure play a role in determining droplet size and frequency of droplet formation.

3. Dimensions of the QDG.

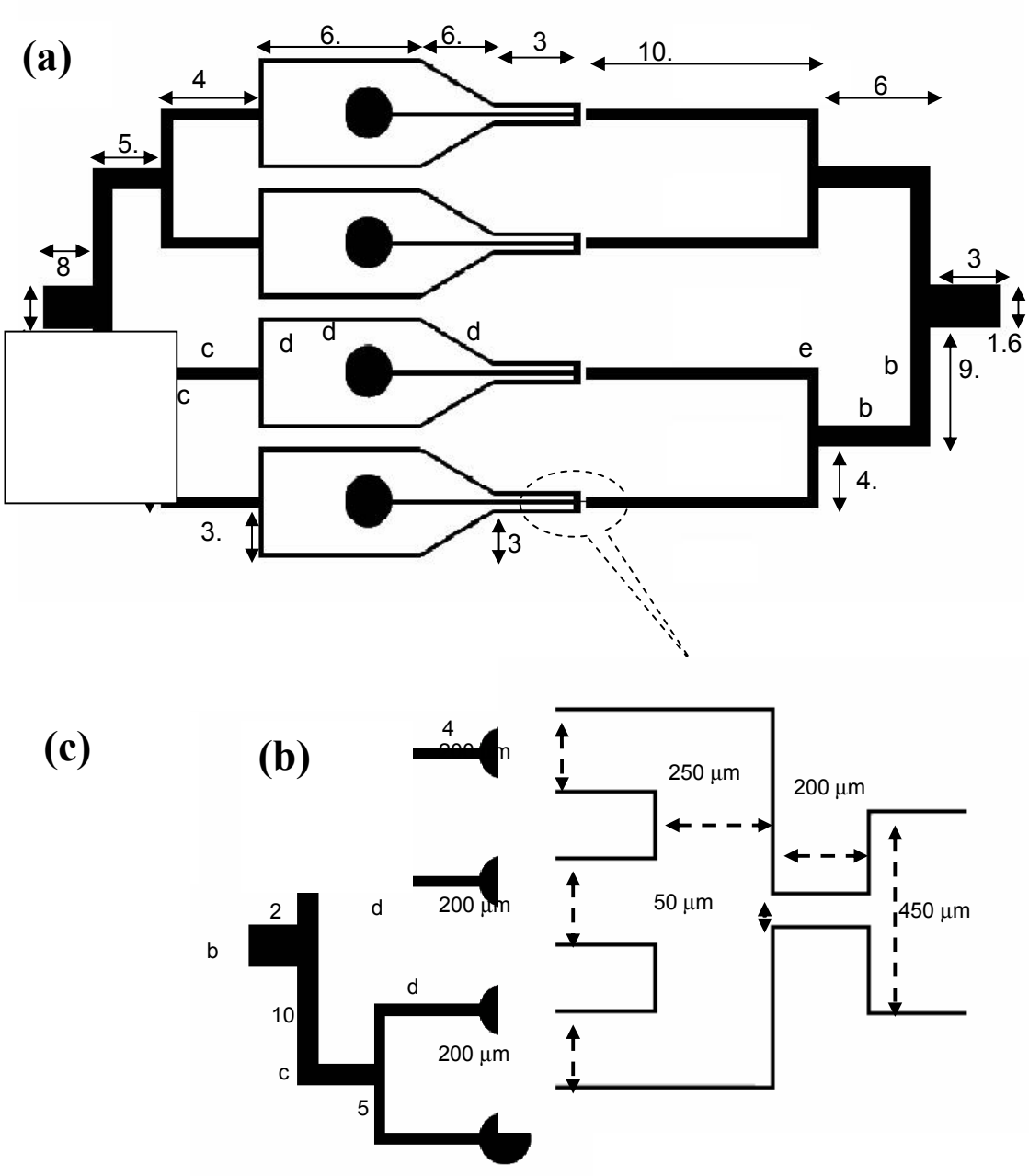

Fig 6. Dimensions of the flow-focusing devices integrated in the QDG. (a,b) Geometry of the devices (a) and the orifice (b) patterned in Sheet 2of the QDG (see Fig 3a). (c) geometry of the device patterned in Sheet 1 (see Fig. 3a). In (a) b= 0.8 mm, c=0.4 mm, d= 0.2 mm, e=0.45 mm

References

1. White, F.M., *Fluid Mechanics, 3rd ed.,* McGraw-Hill, Inc, 1994, pp. 342-348.

2. Shah, R.K., London, A.L., Laminar Flow Forced Convection in Ducts, Adv. Heat Transfer, Supplement I, Academic Press, New York, 1978.

3. Steinke, M.E., Kandlikar, S.G., Single-phase liquid friction factors in microchannels, *Int. J. Thermal Sciences*, 45: 1073-1083 (2006).